American Journal of Chemistry 2025, 15(4): 89-101
DOI: 10.5923/j.chemistry.20251504.02

Elimination of Phosphate Ions by Coupling Adsorption/Electrocoagulation Processes Using Activated Carbon from *Hyphaene thebaica* Kernels and Iron Electrodes

Blaise Kom[1,*], Richard Domga[2], Balike Musongo[3], Romuald Teguia Doumbi[1], Lys Carelle Motue Waffo[1], Bruno Fachakbo[1], Serge Raoul Tchamango[1]

[1]Department of Chemistry, Faculty of Science, University of Ngaoundere, Ngaoundere, Cameroon
[2]Department of Applied Chemistry, National School of Agro Industrial Sciences, University of Ngaoundere, Ngaoundere, Cameroon
[3]Department of Chemical Engineering, School of Chemical Engineering and Mineral Indistries, University of Ngaoundere, Ngaoundere, Cameroon

Abstract In this work, phosphate ions were removed from aqueous solutions through adsorption (AD) with activated carbon (AC), electrocoagulation (EC) with iron electrodes, and both processes combined (adsorption and electrocoagulation). Batch mode adsorption experiments were conducted to evaluate the influence of certains parameters, including solution pH, adsorbent dosage, time contact, and initial phosphate concentration. The results of adsorption process showed that maximum phosphate ions removal was reached after 20 minutes, and under acidic conditions. This removal increased with the increase of initial phosphate concentration while decreasing with increased adsorbent dosage. The maximum adsorption capacity of AC for phosphate was determined to be 16.24 mg/g. Kinetics data analysis revealed that phosphate ions adsorption followed a pseudo-second order model. During electrocoagulation process, various operational parameters were investigated, including current intensity, initial phosphate concentration, initial pH, supporting electrolyte concentration, and electrolysis time. The obtained results showed that 97.14% of phosphate ions were eliminated under optimal conditions: 50 minutes duration, 100 mA current intensity, 40 mg/L initial phosphate concentration, pH 9, and 2g/L NaCl concentration. The coupling of AD/EC and EC/AD processes in two simultaneous steps was also examined, with time being the only parameter varied. The obtained results leaded to 99.58% phosphate ions removal after 30 minutes of treatment, higher than respective removals of 82.66% and 97.14% by adsorption and electrocoagulation used individually.

Keywords Activated carbon, Adsorption, Electrocoagulation, *Hyphaene thebaica*, Iron electrodes, Phosphates ions

1. Introduction

Water plays a critical role in daily consumption and hygiene needs, serving as an indispensable element for all terrestrial life forms. Moreover, water is vital in various industrial processes such as beverage production, food preparation, and sanitation [1], [2], [3]. However, uneven distribution of water resources across agricultural, livestock, mining, washing and industrial sectors poses significant challenges in accessing clean water [4]. Contaminated water sources harbor various harmful compounds that can induce numerous adverse effects on both human health and ecosystem integrity [5]. Nowadays, the use of water becomes a persistent concern for governments, particularly in developing countries. Many diseases are directly linked to water, due by the discharge of untreated wastewater into the environment. Furthermore, industrial and anthropogenic activities are major contributors to water pollution, introducing toxic chemicals such as organic pollutants (e.g. aromatic compounds, pesticides, hydrocarbons) and inorganic pollutants (e.g. nitrates, phosphates, heavy metals like Cr, Pb, Cd, Hg) into aquatic environment [6]. Municipal wastewater, for instance, contains approximately 25 mg/L of phosphates, orthophosphates, and polyphosphates [6]. Elevated concentrations of these pollutants (above 0.20 mg/L) can trigger excessive algae growth, leading to lakes and rivers eutrophication. Eutrophication, caused by an ecosystem receiving an abundance of nutrients such as phosphorus and nitrogen, contributes to degradate water quality and renders it unsuitable for various uses [7]. This degradation has detrimental effects on human health, the environment, and local economic activities [8].

* Corresponding author:
komblaise@yahoo.fr (Blaise Kom)
Received: Oct. 20, 2025; Accepted: Nov. 16, 2025; Published: Nov. 25, 2025
Published online at http://journal.sapub.org/chemistry

Given the need to mitigate water pollution, various treatment methods have been developed, including physicochemical processes (ion exchange, membrane technologies, chemical precipitation) and biological processes (biofiltration, activated sludge, lagoons) [9], [10]. However, these methods often have insufficiencies. For instance, ion exchange and membrane techniques transfer pollutants from the liquid phase to solid phase without destroying them, generating secondary waste at high costs. Chemical precipitation and coagulation require multiple stages, strict pH control, and expensive chemicals, resulting in significant sludge production. Biological methods necessitate sludge removal and treated water disinfection, also contributing to secondary pollution [11]. Given these limitations, we have chosen environmentally-friendly processes: activated carbon adsorption and electrocoagulation. These processes are simpler, less expensive, less restrictive, and utilize locally available waste materials. Activated carbon adsorption is noted for its large surface area, micro porous structure, and high pollutant adsorption capacity, although industrial activated carbon's cost and regeneration challenges limit its widespread application [12]. Consequently, recent studies have explored the feasibility of using activated carbon derived from natural materials such as agricultural and industrial waste for pollutant removal [13], [14], [15]. In this study, activated carbon will be produced from agricultural waste (HT) core shells.

Electrocoagulation is an electrochemical process with sacrificial soluble aluminium or iron anodes. In this process, the action of a convenient current frees metal ions (Al^{3+}, Fe^{2+} or Fe^{3+}) by anode oxidation. These ions combine then with hydroxyl ions released at the cathode, leading to aluminium or iron hydroxides and enhance flocks formation [16], [17]. When iron electrodes are used, the following mechanisms could explain the observed phenomena [16], [18], [19].

Mechanism 1

At the anode:

$$4Fe \rightarrow 4Fe^{2+} + 8e \quad (1)$$

In the solution:

$$4Fe^{2+} + 10H_2O + O_2 \rightarrow 4Fe(OH)_3 + 8H^+ \quad (2)$$

At the cathode:

$$8H^+ + 8e \rightarrow 4H_2 \quad (3)$$

The overall reaction:

$$4Fe + 10H_2O + O_2 \rightarrow 4Fe(OH)_3 + 4H_2 \quad (4)$$

Mechanism 2

At the anode:

$$Fe \rightarrow Fe^{2+} + 2e \quad (5)$$

In the solution

$$Fe^{2+} + 2OH^- \rightarrow Fe(OH)_2 \quad (6)$$

At the cathode:

$$2H_2O + 2e \rightarrow 2OH^- + H_2 \quad (7)$$

The overall reaction:

$$Fe + 2H_2O \rightarrow Fe(OH)_2 + H_2 \quad (8)$$

Electrocoagulation offers advantages such as automation potential, high efficiency, and reduced chemical uses, easily accessible electrodes (iron or aluminum) and combines coagulation-flocculation, adsorption, flotation, and electrochemistry processes, making it effective against a wide range of pollutants [10], [20]. Moreover, electrocoagulation can operate using sustainable energy sources like wind, solar, and fuel cells [21].

Previous works showed that combining adsorption and electrocoagulation process enhanced the efficacy of treatment in treating complex pollutants from real wastewater [22], [23]. Despite these advantages, the synergistic use of adsorption and electrocoagulation processes, particularly in treating phosphate ions, remains unexplored. Therefore, this study aims to investigate the removal of phosphate ions from aqueous solutions activated carbon adsorption and electrocoagulation processes individually, followed by a hybrid adsorption-electrocoagulation (AD-EC) system.

Phosphorus is a non-metallic element that is widely present in domestic, industrial, and agricultural wastewater. In surface water, it contributes to eutrophication and is generally found in the form of stable ions such as orthophosphates (PO_4^{3-}) and polyphosphates (inorganic phosphates) in water or in organic molecules (organic phosphates). It can therefore occur in the form of free ions or chemically bound to organic matter, making it difficult to remove using a single method (adsorption or electrocoagulation), hence the interest in combining adsorption and electrocoagulation to remove phosphorus from water.

The AD-EC combination allows for more efficient and complete removal of pollutants, particularly those that are difficult to treat with a single method, such as phosphorus. It also allows for the treatment of a wide range of pollutants, including heavy metals, dissolved organic matter, and refractory compounds, which can be difficult to remove with a single method. The combination allows the treatment to be adapted to the specific characteristics of the effluent, significantly reducing turbidity and chemical oxygen demand.

The study will involve the preparation and characterization of activated carbon derived from *Hyphaene thebaica* core shells (CA-HT), evaluation of phosphate ion removal efficiency through adsorption and electrocoagulation, and assessment of time-dependent effects in the AD-EC hybrid system for phosphate ion removal from aqueous media.

2. Materials and Methods

2.1. Chemicals and Reagents

All chemicals used in this study were of analytical grade (NaCl, 99%; NaOH, 99%; H_2SO_4, 96%, $(NH_4)_2MoO_4$, 98%

C_6H_8O, 99% and KH_2PO_4, 98%). The synthetic wastewater in this study was prepared from KH_2PO_4. Test solutions were prepared using ultra-pure Milli-Q water (Millipore, resistivity > 18 MΩ cm).

2.2. Adsorbent Materials

To convert local materials into activated carbon, *Hyphaene thebaica* (HT) core shells were used as the adsorbent. Fruits of HT were sourced from the local market. The fruits were peeled, washed with tap water, dried for 4 days, and then crushed to separate the shells from core. The shells were collected for further processing. Figure 1 illustrates different parts of these fruits.

2.3. Preparation of Activated Carbon

The core collected previously were ground and sieved to retain fractions less than 200 µm, then dried in an oven at 105 ℃ for 24 hours. The preparation proceeded in three main stages: Carbonization (pyrolysis) of the ground biomass at 600 ℃ in a programmable Nabertherm muffle furnace with a heating rate of 2.5 ℃/min for 3 hours. The resulting material was cooled to room temperature and then impregnated with ortho-phosphoric acid solution. After stirring for 24 hours at room temperature using a Mivar Magnetic Stirrer, the impregnated material was filtered, washed with distilled water until reaching a constant pH (measured using a HANNA HI 2209 pH meter), and dried in an oven at 105 ℃ for 24 hours. The dried material was subsequently cooled in a desiccator for 24 hours [24].

2.4. Characterization of Activated Carbon

Physicochemical tests included determination of pyrolysis yield, ash content, moisture content, adsorption capacity and specific surface area were carried out on the prepared activated carbons to evaluate their quality and performance.

2.4.1. Pyrolysis Yield

The pyrolysis yield, expressed as a percentage, reflects the mass loss during pyrolysis and was calculated using Equation 9.

$$R\ (\%) = \frac{m_i - m_f}{m_i} \times 100 \quad (9)$$

m_i: Initial mass of the coal;
m_f: Final mass of the coal.

2.4.2. Dry matter Content

The dry matter content was determined following [25] standards by drying a sample at 105 ± 2 ℃ until a constant weight was achieved. The dry matter content (DM) is calculated using Equation 10.

$$DM\ (\%) = 100 - \frac{p_1 - p_2}{p_1} \times 100 \quad (10)$$

P_1: weight (g) of the crucible filled with powder before drying;
P_2: weight (g) of the crucible filled with powder after drying.

2.4.3. Ash Content

Ash content (AC) was determined according to [25] by heating a sample in an oven and calculating the ash content using Equation 11.

$$AC(\%) = \frac{p_1 - p_0}{p_1} \times 100 \quad (11)$$

P_0: weight (g) of the crucible before carbonization;
P_1: weight (g) of the crucible after carbonization.

2.4.4. Iodine Index

The iodine index, a measure of the adsorbent's ability to adsorb small molecules, was determined according to AWWA B 600-78 standard [26]. The iodine index is calculated using Equation 12.

$$\text{Iodine Index (mg/g)} = \frac{(C_o - \frac{C_{th} V_{th}}{2VI_2}) M_{I_2} V_{ads}}{m_c} \quad (12)$$

C_0: Initial concentration of iodine solution (mol/L).
C_{th}: Concentration of sodium thiosulfate solution (mol/L);
V_{th}: Volume of thiosulfate poured to the equivalence (mL);
V_{I_2}: Volume of iodine measured (mL);
M_{I_2}: Molar mass of iodine (g/mol);
V_{ads}: Adsorption volume (mL);
m_c: Mass of adsorbent (g).

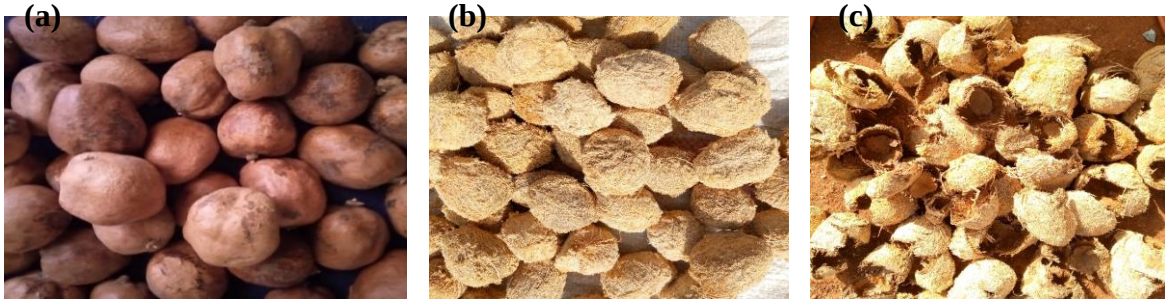

Figure 1. *Hyphaene thebaica* **(a)** fruits, **(b)** peeled fruits, **(c)** stone shells.

2.4.5. Determination of Methylene Blue (MB) Index

The methylene blue index (Q_{MB}) was used to evaluate the macroporosity and mesoporosity of activated carbons. The MB index was calculated using Equation 13.

$$Q_{MB} = \frac{(C_i - C_r)\times V}{m_{ca}} \times 100 \quad (13)$$

Q_{BM}: Adsorption capacity (mg/g);
C_i: Initial concentration of the MB solution (mol/L);
C_r: Residual concentration of MB solution (mol/L);
V: Volume of MB solution (mL);
m_{ca}: Mass of AC used (g).

2.4.6. Specific surface

The specific surface (SS) area was estimated based on the adsorption capacity of the adsorbent for a given solute, calculated using Equation 14.

$$SS = \frac{Q_{max}\times S\times N_A}{M_{BM}} \quad (14)$$

Q_{max}: Maximum adsorption capacity (mg/g);
S: Area occupied by a MB molecule (175 Å^2);
N_A: Avogadro number;
M_{MB}: Molar mass of MB (319.853 g/mol).

2.4.7. pH at Point of Zero Charge (pH_{ZPC})

The pHZPC was determined using the solid addition method with NaCl solutions at different pH values, and the pH was measured after stirring for 24 hours [27].

2.4.8. Fourier Transformed Infrared Spectroscopy (FTIR)

FTIR spectroscopy was employed to identify functional groups in raw and activated *Hyphaene thebaica* materials.

2.5. Batch Adsorption Experiments

Adsorption capacity of activated carbon (AC) was evaluated by mixing AC with phosphate ions solution, followed by filtration and UV-visible spectrophotometry analysis to determine residual phosphate ions concentrations. Adsorption capacities were obtained using Equation 15.

$$q_e = \frac{(C_0 - C_e)\,V}{m} \quad (15)$$

q_e: Equilibrium adsorption capacity per ram dry weight of the adsorbent (mg/g);
C_0: Initial concentration of PO_4^{3-} (mg/L);
C_e: Final concentration of PO_4^{3-} (mg/L);
V: Volume of the solution (L);
M: Mass of the adsorbent (g).

2.6. Modeling of Adsorption Kinetics

Pseudo-first order model: The pseudo-first order model was applied to describe adsorption kinetics using Equation 16 and 17.

$$\frac{dqt}{dt} = K_1(q_e - q_t) \quad (16)$$

$$\ln(q_e - q_t) = \ln(q_e - K_1 t) \quad (17)$$

K_1: Rate constant of the pseudo first order model (min^{-1});
q_t and q_e: Adsorption capacities, respectively at time t and at equilibrium (mg/g).

Pseudo-second order model: The pseudo-second order model was used to characterize chemisorption kinetics using Equation 18 and 19.

$$\frac{d_{q_t}}{dt} = K_2(q_e - q_t)^2 \quad (18)$$

$$\frac{t}{q_t} = \frac{1}{K_2 q_e^2} + \frac{t}{q_e^2} \quad (19)$$

K_2: Rate constant for second order kinetics expressed (g.mg^{-1}.min^{-1});
q_t et q_e: Adsorption capacities, respectively at time t and at equilibrium (mg/g).

2.7. Adsorption isotherms

The Langmuir isotherm model was employed to analyze the adsorption equilibrium data using Equation 20 and 21 and the Freundlich isotherm model was used to describe multilayer adsorption using Equation 22 and 23.

$$q_e = \frac{q_{max}\cdot K_L\cdot C_e}{1+K_L\cdot C_e} \quad (20)$$

$$\frac{C_e}{q_e} + \frac{1}{q_{max}\times K_L} + \frac{C_e}{q_{max}} \quad (21)$$

C_e: Concentration at equilibrium (mg/L);
q_e: Quantity adsorbed at equilibrium (mg/g);
q_{max}: Maximum adsorption capacity (mg/g);
K_L: Langmuir equilibrium value (L/mg).

$$q_e = K_{F.}\, C_e^{\,1/n} \quad (22)$$

$$Log_{q_e} = Log_{K_L} + \frac{1}{n} Log_{c_e} \quad (23)$$

q_e: Adsorbed quantity (mg/g);
C_e: Balance concentration (mg/L);
K_F and n: Freundlich constants associated with adsorption capacity and adsorption affinity and adsorption affinity, respectively (L/g).

2.8. Electrocoagulation

2.8.1. Electrochemical Reactor

A 250 mL beaker was used as reactor during the experiments (Figure 2). The volume of effluent to be treated was 200 mL. Two iron electrodes of the same size were used, each with a length of 5 cm and a radius of 0.5 cm. They were positioned 2 cm apart a distance chosen to minimize ohmic drop yet sufficient to prevent clogging and ensure effective agitation. Before electrolyses, NaCl was added to the solution to ensure the conductivity of the medium. The pH of the solutions was adjusted by adding NaOH and H_2SO_4 (0.1 N).

Prior to electrocoagulation experiments, operational parameters such as current intensity, initial pollutant concentration, electrolysis duration, initial pH of the effluent, and supporting electrolyte concentration were investigated. After electrocoagulation experiments, the electrodes were removed from the reactor and cleaned with a 0.1 N sulfuric

acid solution to eliminate pollutant deposits that could form resilient layers on the electrode surface.

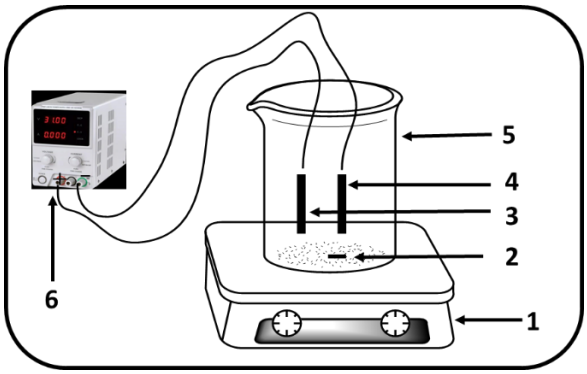

Figure 2. Electrochemical device: 1-Magnetic stirrer, 2-Magnetic bar, 3-Anode (Iron), 4-Cathode (Iron), 5-Electrochemical cell, 6-D.C power supply

2.8.2. Analytical Measurements

The titration of phosphate ions was conducted using UV-Visible spectrophotometry. The residual phosphate concentration was determined after the formation of a phosphomolybdic complex. In acidic medium and in the presence of ammonium molybdate, orthophosphates form a phosphomolybdic complex, which, when reduced by ascorbic acid, develops a blue color [28]. The efficiency of phosphate ion removal was determined using Equation 24 and the desorption efficiency (DE) using Equation 25.

$$\%EE = \frac{C_i - C_f}{C_i} \times 100 \quad (24)$$

$$DE = \frac{C_{des_e} \times V_{des}}{(C_{ads_0} - C_{ads_e}) V_{ads}} \times 100 \quad (25)$$

C_i: Initial concentration of PO_4^{3-} (mg/L);
C_f: Final concentration of PO_4^{3-} (mg/L);
EE: Removal efficiency (%);
C_{des_e}: Concentration of phosphate ions desorbed at equilibrium (mg/L);
C_{ads_0} : Initial concentration of phosphate ions (mg/L);
V_{ads}: Volume of adsorption solution (L);
V_{des}: Volume of desorption solution (L).

2.9. Coupling of Adsorption/Electrocoagulation Processes

The coupling was carried out by introducing, which stirring the activated carbon into the electrocoagulation reactor containing the solution to be treated. After adsorption, the electrocoagulation process was carried out. Furthermore, another coupling was carried out by first performing electrocogulation, followed by the actived carbon adsorption process.

3. Results and Discussion

3.1. Adsorption Process

3.1.1. Physico-chemical Characteristics of Activated Carbon

Table 1 presents the physicochemical characteristics of the activated carbon used in this study. The activation yield of 83.12% indicates a loss of 16.88% of the carbonaceous material (CA), attributed to the washing process with distilled water to remove activating agents. In fact, during washing, some carbon particles clog filter paper while others are carried away by rinsing water.

Moisture content, representing the amount of free water in the material, is crucial as it varies with pore structure. The adsorbent exhibits low moisture content (0.15%), suggesting a predominance of micropores which adsorb minimal water and enhance adsorption capacity [29]. The high dry matter content (99.88%) indicates an organic composition similar to [29].

The value of ash content, indicates that the inorganic fraction, is low (1.18%), confirming the predominance of carbon. Lower ash content obtained indicated higher quality activated carbon.

The iodine number and methylene blue index are crucial indicators of adsorption performance in micropores and mesopores, respectively. An iodine number above 900 mg/g is ideal for effective adsorption of small molecules [30]. Obtained results (399.74 mg/g) indicate relatively low microporosity compared to previous studies [31], while the MB index (46.32 mg/g) suggests a combined micro and mesoporous structure, suitable for adsorbing contaminants of various sizes.

The specific surface area obtained (321.03 m^2/g) is lower compared to similar studies using *Hyphaene thebaica* precursor [31], [32], indicating differences in activation processes and precursor materials.

Table 1. Physicochemical characteristics of activated carbon

Features	Values
Activation performance (%)	83.12 ±0.01
Moisture content (%)	0.15 ±0.05
Dry matter content (%)	99.88 ±0.05
Ash content (%)	1.18±0.58
Iodine index (mg/g)	399.74 ±0.95
Methylene blue index (mg/g)	46.32 ±0.19
Specific surface (m^2/g)	321.03 ±0.02

3.1.2. pH at Point of Zero Charge (pH_{PZC})

The pH at the point of zero charge (pH_{PZC}) provides information regarding the adsorbent's surface charge. It is the pH value of the solution where the net charge on the surface becomes zero, balancing the positive and negative charges. The adsorption of molecules or ions onto a solid surface is significantly influenced by the pH of the medium, particularly at the pH_{PZC} where the surface charge is neutral. Figure 3.a illustrates the pH point of zero charge (pH_{PZC}). According to Figure 3.a, the pH_{PZC} of the activated carbon (AC) is 5.9. This pH value indicated that the surface charge of the AC becomes neutral. Consequently, for adsorbates

with pH values below the pH_{PZC} (pH < 5.9), the surface of the produced carbonaceous adsorbent (CA) is positively charged, thereby favoring the adsorption of anionic species. Conversely, for solute pH values above the pH_{PZC} (pH > 5.9), the CA surface carries negative charges, which promotes the adsorption of cationic species. The pH_{PZC} value of 5.9 closely matches that reported by [31] using the same precursor, HT, who obtained a pH_{PZC} of 6.

3.1.3. Fourier Transformed Infrared Spectroscopy (FTIR)

Fourier Transformed Infrared Spectroscopy (FTIR) is a crucial analytical technique utilized for identifying characteristic functional groups involved in adsorption chemistry. Figure 3.b presents the FTIR spectrum of coal-based shells derived from *Hyphaene thebaica* cores.

The prominent absorption bands at (407.56 - 565.80) cm^{-1} are attributed to the stretching vibration of –OH. The peak at 1428.43 cm^{-1} corresponded to the stretching vibrations of $–CH_2$. The band observed at approximately 1681.52 cm^{-1} is indicative of –COOH, while the peak around 1375.29 cm^{-1} is associated to phenol group. The characteristic peak at 889.92 cm^{-1} is attributed to the C–O bending vibration in –COH. The band at approximately 752.26 cm^{-1} was related to the out-of-plane bending mode of O–H. The range (2250-2400) cm^{-1} corresponded to the C≡C stretching vibration, characteristic of alkyne group. Overall, the AC surface exhibits abundant functional groups, particularly –OH, –COOH, and –COH. These polar functional groups enhanced the adsorption of polar solutes. The presence and enhancement of these functional groups in the adsorption capacities of AC corroborated the findings of [33].

3.1.4. Influence of Adsorption Parameters

3.1.4.1. Influence of Time Contact

The influence of contact time on phosphate ion adsorption was studied at room temperature with 0.10 g of adsorbent and a solution concentration of 6.00 mg/L of PO_4^{3-}. Figure 4.a illustrates the time-dependent adsorption process. Two distinct phases were observed: an initial rapid increase in adsorbed phosphate quantities from t = 0 min to t = 20 min, attributed to the availability of vacant active sites and strong affinity between phosphate ions and the adsorbent [34]. Subsequently, from t = 30 min to t = 60 min, a plateau phase was observed, indicating the saturation of the adsorption sites on the activated carbon surface. The equilibrium time for phosphate ion adsorption was determined to be 20 minutes, achieving adsorbed quantities of 15.47 mg/g and 16.24 mg/g from an initial concentration of 6.00 mg/L.

3.1.4.2. Influence of Initial Concentration of Phosphate Ions

The effect of initial phosphate ion concentration on adsorption is depicted in figure 4.b. As seen in this figure, higher initial concentrations resulted in the increase the quantity of adsorbed phosphate ions, with adsorption rising from 0.83 mg/g to 2.03 mg/g as concentration increases from 2.00 mg/L to 10.00 mg/L. This phenomenon is attributed to greater availability of phosphate ions and their stronger driving force toward adsorbent sites [35]. A concentration of 6.00 mg/L is used for further study, as beyond this concentration, adsorbed quantities of phosphate ions show minimal variation.

3.1.4.3. Influence of Activated Carbon Mass

Figure 4.c depicts the influence of adsorbent mass on adsorbed phosphate quantities. Increasing adsorbent mass initially increases adsorption, but beyond 0.10 g, the curve representing adsorbed quantities reaches a plateau, indicating saturation of active sites and reduced accessible surface area due to particle agglomeration [36]. The adsorbed quantities decrease from 62.71 mg/g to 7.89 mg/g, Starting at 0.1 g of activated carbon, the amounts of adsorbed phosphate ions hardly vary anymore.

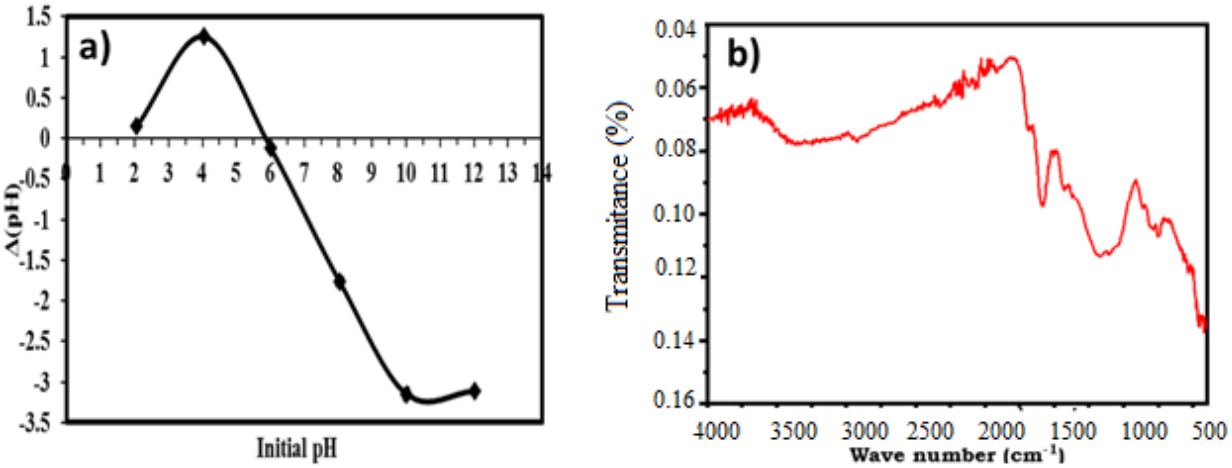

Figure 3. **a)** Zero Charge Point pH (pH_{ZPC}) of AC derived from *Hyphaene thebaica* core shell, **b)** FT-IR spectrum of AC

3.1.4.4. Influence of pH During Adsorption

Figure 4.d shows the influence of solution pH on adsorbed phosphate quantities. As shown in this figure, maximum adsorption occured at pH 6, attributed to electrostatic attraction and ion exchange between phosphate ions and the carbon surface [40]. At lower pH, positively charged surface sites dominated, facilitating phosphate ion adsorption via electrostatic forces. At pH > 6, competition between phosphate ions and hydroxyl ions (OH^-) for adsorption sites reduces phosphate adsorption. The optimal pH of 6 corresponds to the point of zero charge (pH_{ZPC}) of the adsorbent, where surface neutrality enhances adsorption efficiency due to minimized electrostatic interactions and increased availability of active sites [39].

3.1.5. Modeling of Adsorption Kinetics

To better describe the adsorption mechanism of phosphate ions on activated carbon (AC), two kinetic models were applied to these experimental data: The pseudo first-order model and the pseudo second-order model. These models elucidate the variation in solute quantity adsorbed on a solid support over time, aiming to identify the mechanisms governing adsorption rate. Figures 5.a-b and Table 2 demonstrate that both orders kinetic models (pseudo first-order and pseudo second-order) are applicable for phosphate ions retention across various ion concentrations. This is supported by high correlation coefficients ($R^2 = 0.97 > 0.95$) (Figure 5.b). Additionally, the calculated adsorbed quantity closely matches experimental results, further validating the applicability of these models for phosphate ion retention on our adsorbent.

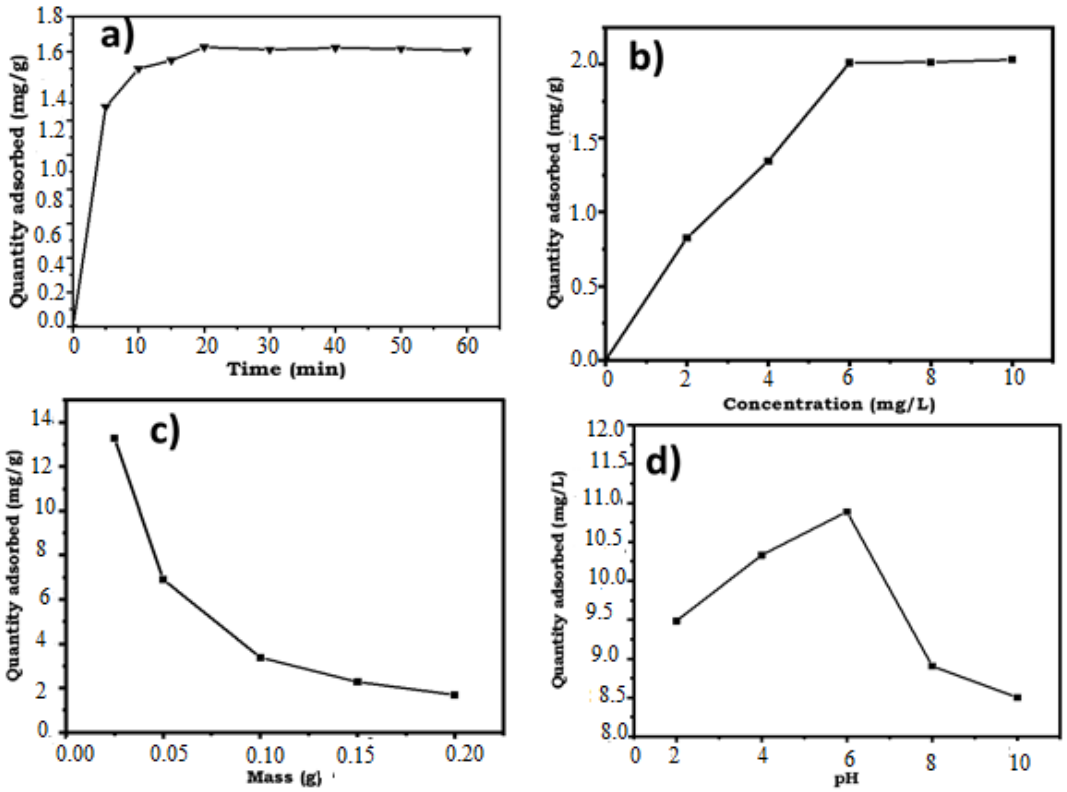

Figure 4. a) Influence of contact time on phosphate removal on activated carbon (AC). b) Effect of initial concentration on the adsorption of phosphate ions by AC. c) Influence of the dose of AC on phosphate ion adsorption. d) Influence of pH on phosphate ion adsorption (pH = (2-10), C=6.00 mg/L, m=0.10g, t=20 min, V=250 rpm)

Table 2. Values of the constants of the pseudo first-order and pseudo second-order kinetic models

Adsorbate	Pseudo-first-order				Pseudo-second order			
	$q_e$exp (mg/g)	$q_e$cal (mg/g)	K_1 (min^{-1})	R^2	$q_e$exp (mg/g)	$q_e$cal (mg/g)	K_2 (g/mg.min)	R^2
PO_4^{3-}	16.243	3.252	0.124	0.647	16.243	16.31 3	0.106	0.975

Table 3. Values of the constants of the Langmuir and Freundlich phosphate adsorption isotherm models

Adsorbent	**Langmuir**				**Freundlich**		
	q_m(mg/g)	K_L(L/mg)	R^2	R_L(mg/L)	n_F(L/mg)^n	K_F(mg/g)	R^2
AC	3.8491	0.5889	0.989	0.3060	3.4482	4.8124	0.9107

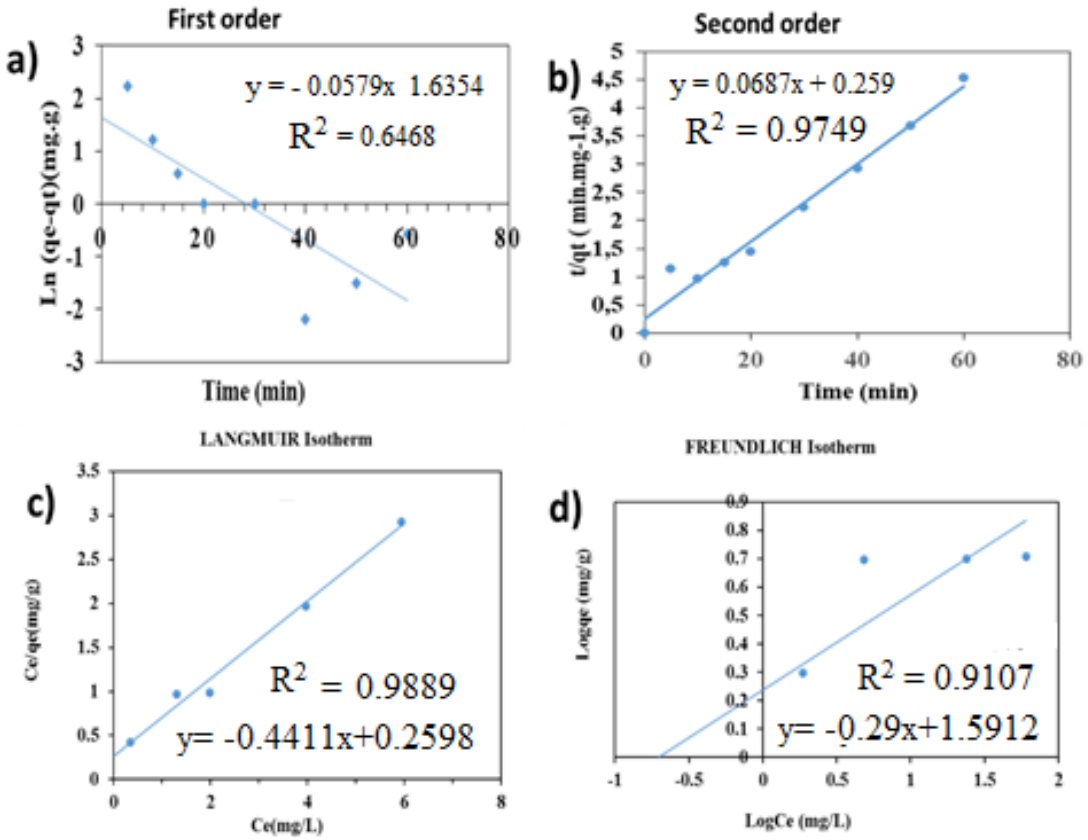

Figure 5. a) Linear representation of the pseudo-first and b) pseudo-second order kinetic model of phosphate ions. Modeling of phosphate adsorption isotherms on AC using the c) Langmuir and d) Freundlich models

3.1.6. Modeling of Adsorption Isotherms

The experimental results were modeled by two isothermal theoretical models to describe the equilibrium adsorption process: Langmuir and Freundlich models. The values of correlation coefficients R^2 and the constants characterizing the adsorption equilibrium of phosphate ions on the AC for two models (Langmuir and Freundlich) are presented in Table 3 and Figures 5.c-d. From this table, it appeared that Langmuir model was more appropriate the Freundlich one for describing the adsorption of phosphate ions with a better correlation coefficient (R^2 >0.95). On the other hand, the R_L value is between 0 and 1, thus proving a good adsorption capacity of the adsorbent and a favorable adsorption reaction. According to the Langmuir model, the KL value indicated that there is adsorption of phosphate with the formation of a monolayer on the adsorbent surface. This involved localized adsorption on well-defined adsorbent sites, likely to bind only a single molecule [40].

3.2. Influence of Parameters on Electrocoagulation

3.2.1. Influence of Current Intensity

Current intensity is a pivotal factor in electrocoagulation and is directly controllable [23]. So, a series of tests were conducted with current intensities ranging from 100 mA to 400 mA, while keeping other parameters constant. As shown in Figure 6.a, phosphate removal efficiency exhibited similar trend, characterized by rapid increase in phosphate removal during the first ten minutes, whatever the imposed current. After 30 minutes of electrocoagulation, a plateau is observed in all the curves. Then more than 85% phosphate removal was eliminated, when the imposed current was 200, 300 and 400 mA. This was not surprising, because according to Faraday's the increase of the current intensity produces a great amount of ferrous and ferric ions are electro-generated and formed hydroxide compounds capable to fix pollutants [19].

3.2.2. Influence of Initial Phosphate (PO_4^{3-}) Concentration

Studying the influence of initial phosphate concentration assessed the process's capability to remove high levels of phosphate ions. Experiments were conducted using phosphate solutions with concentrations of 10, 20, 30, 40, and 50 mg/L. Figure 6.b shows that all concentration curves exhibited similar behavior: rapid reduction followed by a plateau. Notably, the reduction is fastest at 10 minutes for all initial concentrations except at 50 mg/L, where phosphate removal rates increase over time before reaching a plateau. At high initial concentrations (50 mg/L), phosphate elimination rates are lower. Treating solutions with higher initial concentrations requires longer reaction times to achieve complete phosphate removal [23].

3.2.3. Influence of pH During Electrocoagulation

To investigate the impact of pH on phosphate removal, experiments were conducted at following pH: 3, 5, 6, 8, and 9. Previous works explained mechanisms occurring during phosphate elimination when iron is used as electrode material [41], [42]. It has been shown that $FePO_{4(s)}$ is formed in the low pH range (<6.5) and in the high pH range (>6.5). $FePO_{4(s)}$ has minimum solubility within pH range of 4.5–5.5, but its solubility increases with increasing pH according to following reactions [41], [43], [44].

$$Fe^{3+} + PO_4^{3-} \rightarrow FePO_{4(s)} \quad (27)$$

$$2Fe^{3+} + 2PO_4^{3-} \rightarrow Fe_3(PO_4)_{2(s)} \quad (28)$$

$$xFe^{3+} + PO_4^{3-} + (3x-3)OH^- \rightarrow Fe_xPO_4(OH)_{3x-3(s)} \quad (29)$$

Here pH significantly influences phosphate removal, with optimal efficiency observed at pH 9, achieving 86.50% removal. In contrast, efficiency at pH 3 was lower, approximately 71.15%. This aligned with previous studies, which suggest that at pH 9, phosphate ions predominantly precipitate as insoluble iron (III) phosphate $FePO_4$, facilitating easy separation by decantation or filtration [45].

The mechanism involves the oxidation of ferrous ions (Fe^{2+}) on the anode surface to ferric ions (Fe^{3+}), which subsequently react with phosphate ions (PO_4^{3-}) to form insoluble iron (III) phosphate. This precipitation reaction was favored at higher pH levels due to reduced competition from hydrogen ions (H^+), which otherwise would form phosphoric acid (H_3PO_4) and inhibit phosphate ion availability for precipitation.

3.2.4. Influence of Supporting Electrolyte Concentration

The conductivity of the reaction medium was varied by adding NaCl, this salt being used as supporting electrolyte. Figure 6.d illustrates the influence of medium conductivity on phosphate elimination during electrocoagulation (EC). The curves in Figure 6.d showed similar trend, initially increasing and stabilizing between 30 and 50 minutes, with phosphate removal efficiency improving with increasing NaCl concentration. NaCl addition enhances current passage through the EC cell, facilitating both electrochemical and chemical dissolution of iron electrodes (Equations 29 and 30). The latter depends on the equilibrium potential of the iron species and the overvoltages (anodic and cathodic).

$$Fe^{3+}{}_{aq} + 3H_2O_{(l)} \rightarrow Fe(OH)_{3(s)} + 3H^+{}_{(aq)} \quad (30)$$

$$Fe(OH)_3 + OH^- \rightarrow Fe(OH)^-{}_{4} + e^- \quad (31)$$

Increasing NaCl concentration improves current density and thus the phosphate elimination rate [46]. Increasing solution conductivity, as explained by [47] reduces the voltage (U) across electrodes at constant current intensity. Conductivity depends on ion concentration, higher electrolyte concentrations increase solution conductivity, enhancing current density and consequently phosphate removal efficiency.

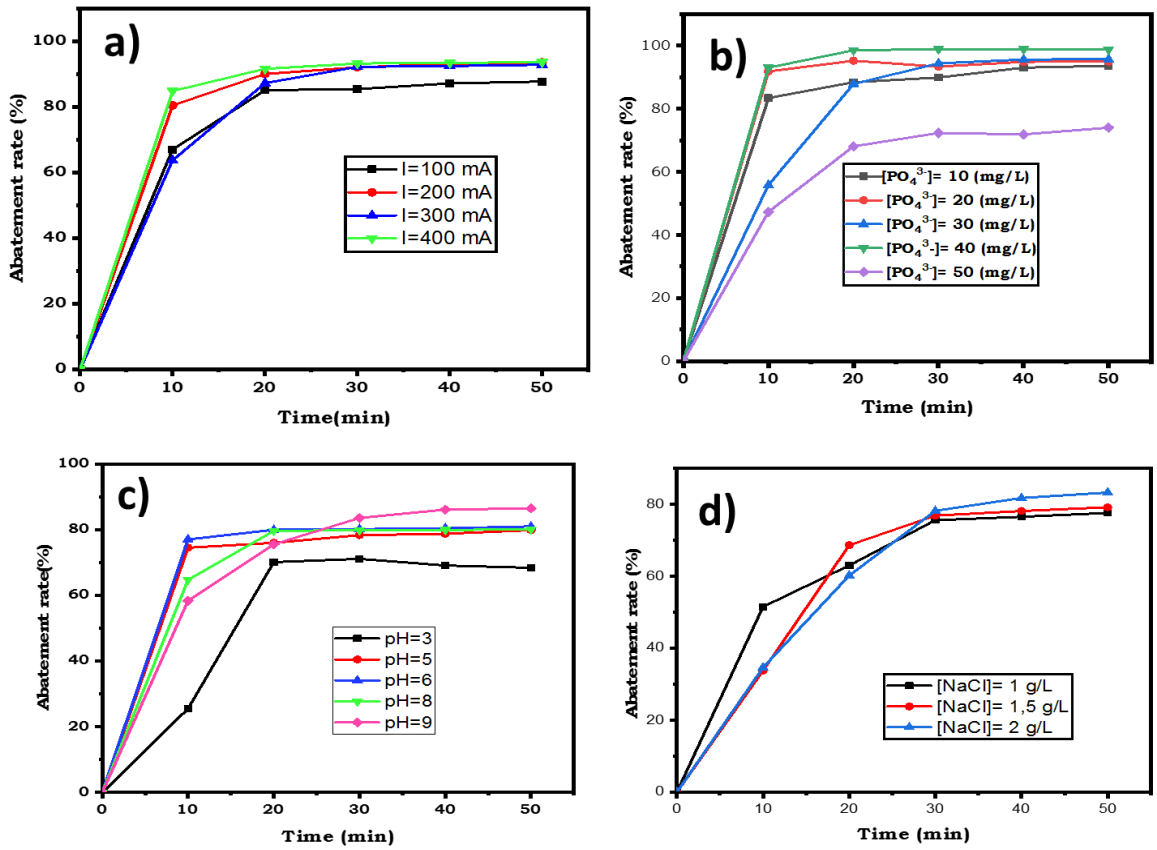

Figure 6. Phosphate reduction rate depending on a) Current intensity, b) Initial phosphate concentration, c) Initial pH of the medium, d) Concentration of the supporting electrolyte-[PO_4^{3-}] = 40 mg/L, V= 200 mL, d =1.5 cm, T= 25 ℃, V= 250 trs/min

3.3. Coupling of Adsorption/Electrocoagulation Processes

When used alone, the adsorption process achieved a phosphate removal rate of approximately 82.66%. In contrast, continuous electrocoagulation with iron electrodes, when used alone, attained an efficiency of approximately 97.14% of phosphate removal. Consequently, it was prudent to explore the combination of these two techniques to further reduce phosphate ions by varying the electrolysis time while maintaining the optimal conditions for both processes.

Table 4. Phosphate Reduction Rates for Coupled Processes

Process	Reduction rate (%)
Adsorption	82.66
Electrocoagulation	97.14
Adsorption / Electrocoagulation	95.74
Electrocoagulation / Adsorption	99.58

Treatment times of 60 minutes were selected in this study based on the results obtained from each process used independently (Figure 7). As shown in Figure 7.a, the coupling effect on phosphate removal was investigated over a range of 0 to 60 minutes, as well as at the optimum conditions for each process. The introduction of the adsorbent material (activated carbon) into the electrocoagulation cell facilitated faster elimination. A total of 99.58% of phosphates were removed within 20 minutes. At the end of the treatment, the phosphate ion reduction rates were highly favorable, approaching 100%. The coupling of adsorption with electrocoagulation (Ads/EC) and electrocoagulation with adsorption (EC/Ads) yielded efficiencies of 95.74% and 99.58%, respectively (Table 4). The enhancement in phosphate ion removal with the addition of activated carbon can be attributed to the simultaneous benefits of both electrocoagulation and adsorption processes. It is evident that phosphate ion removal kinetics are rapid with electrocoagulation. The destabilization of colloids by in situ-generated cations and their adsorption onto metal hydroxide forms contribute to the reduced pollutant elimination time.

Mechanisms can be proposed for each of these complex combined treatment: electrocoagulation (EC) or adsorption on coconut active carbon (CAC), including the corresponding mechanisms, iron electrodes, and reactions involved in EC, as well as the texture of spent coal (surface sites and porosity) [48].

The mechanisms of EC clarification are can be summarized as follows: trapping of phosphate ions within the small clusters of amorphous iron hydroxide flocs formed in excess, and adsorption of phosphate ions on the amorphous iron hydroxides formed. Additionally, destabilization of phosphates can occur through the neutralization of the colloidal surface by the positive species of the coagulant, or through complexation/precipitation, where the positively charged coagulant species can bind to the negatively charged phosphates, thus forming a $Fe(PO_4)_3$ precipitate which can be removed through the separation process [49]. The removal of phosphates can be attributed to the synergistic effect of both the EC process and the adsorption process.

3.4. Regeneration of Adsorption Sites

The regeneration of the activated carbon adsorption sites is performed using an aqueous solution of sodium chloride (NaCl) with a concentration of 4.00 g/L and a pH of 6. The study involved treating 100 mL of sodium chloride solution, containing 0.10 g of phosphate ions, under magnetic stirring (250 rpm) at room temperature. Figure 7.b illustrates the quantity desorbed as a function of time. It can be observed that initially, desorption curve decreases rapidly with stirring time. Then, between 40 and 50 minutes, the curve increases and subsequently decreases again at 60 minutes. This behavior can be explained by the large release of phosphate ions initially adsorbed by the activated carbon at the start beginning of the experiment. After 40 and 50 minutes, the release of ions into the medium began, and at 60 minutes, the regeneration process restarted.

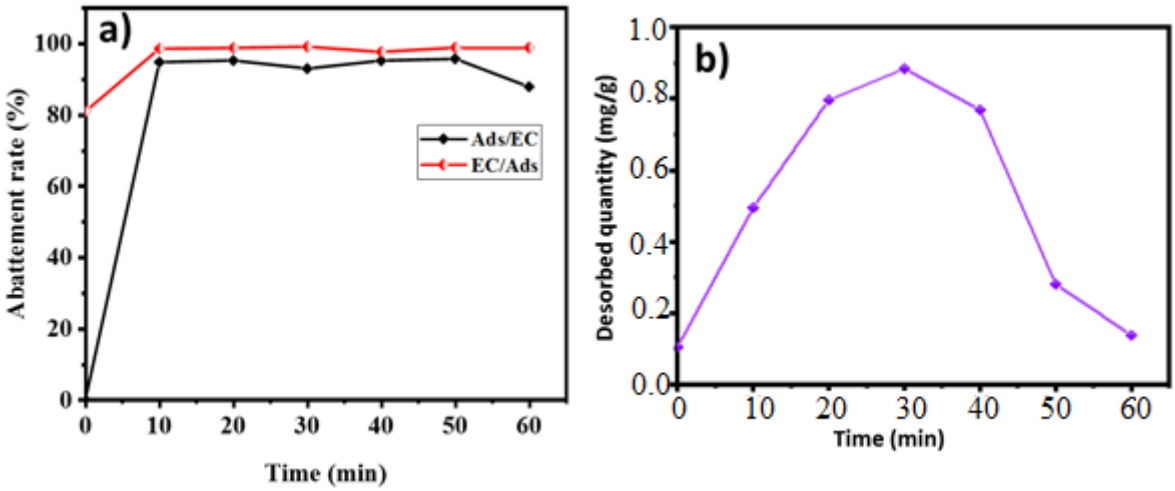

Figure 7. a) Phosphate reduction rate by Ads/EC and EC/Ads as a function of time, b) Kinetics of desorption of phosphate ions previously retained on activated carbon. I=100 mA, pH=6, m=4.00 g/L, $[PO_4^{3-}]$ = 6.00 mg/L, [NaCl] = 2.00 g/L, V = 200 mL, T = 25 ℃; V = 250 trs/min

The quantities of adsorbed and desorbed phosphate ions are provided in Table 5. The analysis of Table 5 indicates that the maximum quantities of desorbed ions were achieved after 30 minutes, corresponding to 0.88 mg/g of PO_4^{3-} initially adsorbed (1.50 mg/g). These desorption results suggest that the phosphate ions were fixed on the surface of the activated carbon in multiple forms, with some being strongly adsorbed and others weakly adsorbed. Consequently, it can be concluded that certain ions were strongly adsorbed via chemisorption, resulting in irreversible adsorption. In contrast, ions that were easily desorbed were weakly adsorbed through physical adsorption, making them more readily desorbable.

Table 5. Values of quantities and desorption rates of phosphate ions

Adsorbant	Q_{ads} (mg/g)	$Q_{dés}$ (mg/g)	$E_{dés}$ (%)
PO_4^{3-}	1.50	0.88	0.10

4. Conclusions

The aim of this study was to remove phosphate ions from an aqueous medium through adsorption onto activated carbon derived from *Hyphaene thebaica* core shells and via electrocoagulation. The physicochemical properties of the adsorbent revealed a combined micro and mesoporous structure, which plays a crucial role in the adsorption process. Infrared (IR) spectroscopy indicated that the adsorbent primarily contains polar functional groups that facilitate the adsorption of polar solutes. The results demonstrated that phosphate ion adsorption onto activated carbon from *Hyphaene thebaica* core shells occurs rapidly within 20 minutes or less. Conversely, the adsorbed quantity decreased with increased mass of the activated carbon. Linear regression analyses revealed that the adsorption kinetics conform to the pseudo-second order model. Langmuir model was observed, with a correlation coefficient greater than 0.95. Electrocoagulation proved effective for treating liquid effluents containing various pollutants. Evaluation of these parameters in the electrocoagulation process indicated that phosphate removal (97.14%) was more efficient than adsorption (82.66%). Combining these two processes achieved a significant removal rate of 99.58%.

Declaration of Competing Interests

The authors declare that there are no conflicts of interest.

Suggestions for Improvement

[1] After 40 and 50 minutes, the release of ions into the medium began. And at 60 minutes, the regeneration process restarted, please explain.

Between 40 and 50 minutes, there is a gradual release of phosphate ions into the medium. This can be explained by competition at the absorption sites, changes in the pH of the medium, ionic strength, and Van der Waals interactions.

[2] Destabilization of phosphates can occur through the neutralization of the colloidal surface by the positive species of the coagulant, why?

The removal of phosphate ions is enhanced in an acidic environment, as the presence of H_3O^+ ions in the environment causes strong interaction with phosphate ions and the acidic functions present on the surface of the activated carbon.

[3] Phosphate ion removal kinetics are rapid with electrocoagulation, explain.

The electrocoagulation process involves several phenomena simultaneously, including the use of current intensity to generate coagulants in situ that cause phosphate ions to agglomerate. Adsorption, on the other hand, requires a single surface reaction that is generally slow and sometimes reversible.

[4] NaCl addition enhances current passage through the EC cell, why?

During electrocoagulation, NaCl increases the conductivity of the electrical current in the medium while reducing electrical resistance and promoting the production of coagulants due to the dissolution of the electrodes.

[5] At high initial concentrations (50 mg/L), phosphate elimination rates are lower. Why?

The rapid saturation of adsorption sites, kinetic factors, and process limitations may explain the low removal of phosphate ions at high concentrations.

REFERENCES

[1] R. M. Kirby, J. Bartram, and R. Carr, "Water in food production and processing : quantity and quality concerns," *Food Control*, vol. 14, no. 5, pp. 283–299, 2003, doi: 10.1016/S0956-7135 (02)00090-7.

[2] Kanu, Ijeoma, and A. O.K., "Industrial Effluents and their Impact on Water Quality of receiving rivers in Nigeria," *J. Applieal Technol. Environ. Sanit.*, vol. 1, no. 1, pp. 75–86, 2011.

[3] K. Valta, T. Kosanovic, D. Malamis, K. Moustakas, and M. Loizidou, "Overview of water usage and wastewater management in the food and beverage industry," *Desalin. Water Treat.*, vol. 53, no. 12, pp. 3335–3347, 2015, doi: 10.1080/19443994.2014.934100.

[4] A. Doggaz, A. Anis, M. M. Le Page, T. Mohamed, and L. François, "No Title," *Sep. Purif. Technol.*, vol. 18, no. 30500–8, pp. 1383–5866, 2018, doi: https://doi.org/10.1016/j.seppur. 2018.04.045.

[5] M. B. Tchamango, S. R., Wandji Ngayo, K., Belibi Belibi, P. D., Nkouam, F., & Ngassoum, "Treatment of a dairy effluent by classical electrocoagulation and indirect electrocoagulation with aluminum electrodes," *Sep. Sci. Technol.*, vol. 56, no. 6, pp. 1128–1139, 2020, doi: https://doi.org/10.1080/01496395. 2020.1748889.

[6] B. S. Rathi, P. S. Kumar, and D. N. Vo, "Critical review on hazardous pollutants in water environment : Occurrence, monitoring, fate, removal technologies and risk assessment,"

Sci. Total Environ., vol. 797, p. 149134, 2021, doi: 10.1016/j.scitotenv.2021.149134.

[7] W. A. Wurtsbaugh, H. W. Paerl, and W. K. Dodds, "Nutrients, eutrophication and harmful algal blooms along the freshwater to marine continuum," *Wiley Interdiscip. Rev. Water*, vol. 6, no. 5, pp. 1–27, 2019, doi: 10.1002/WAT2.1373.

[8] O. Sofia, J. Corburn, and H. Ribeiro, "Challenges regarding water quality of eutrophic reservoirs in urban landscapes: A mapping literature review," *Int. J. Environ. Res. Public Health*, vol. 16, no. 1, 2019, doi: 10.3390/ijerph16010040.

[9] A. R. A. Aziz, P. Asaithambi, and W. M. A. B. W. Daud, "Combination of electrocoagulation with advanced oxidation processes for the treatment of distillery industrial effluent," *Process Saf. Environ. Prot.*, vol. 99, pp. 227–235, Jan. 2016, doi: 10.1016/j.psep.2015.11.010.

[10] X. Liu *et al.*, "Enhanced dyes adsorption from wastewater via Fe3O4 nanoparticles functionalized activated carbon," *J. Hazard. Mater.*, vol. 373, pp. 397–407, Jul. 2019, doi: 10.1016/j.jhazmat.2019.03.103.

[11] M. A. Musa and S. Idrus, "Physical and biological treatment technologies of slaughterhouse wastewater: A review," *Sustain.*, vol. 13, no. 9, pp. 1–20, 2021, doi: 10.3390/su13094656.

[12] Y. Fang, K. Yang, Y. Zhang, C. Peng, and A. Robledo-cabrera, "Highly surface activated carbon to remove Cr (VI) from aqueous solution with adsorbent recycling," *Environ. Res.*, vol. 197, no. 111151, 2021, doi: 10.1016/j.envres.2021.111151.

[13] O. E. Ogwuche, E. C. Gimba, and S. E. Abechi, "An Evaluation of the Adsorptive Behaviour of Activated Carbon Derived from Hyphaene Thebaica Nut Shells for the Removal of Dichlorvos from Wastewater Abstract :," *Int. J. Sci. Technoledge*, vol. 3, no. 4, pp. 274–285, 2015.

[14] G. Wyasu, G. C. E., A. E. B., and N. G. I., "Production and Characterization of Active Carbon from Epicarp of Balanite Aegyptiaca and Detarium Mirocarpum Shells," *Int. J. Sci. Technoledge*, vol. 4, no. 3, pp. 19–25, 2016.

[15] S. Samaila, M. H. Adamu, and J. J. Deshi, "Adsorption of lead and mercury ions on chemically treated doum palm shells," *IDOSR J. Sci. Res.*, vol. 2, no. 1, pp. 25–36, 2017.

[16] S. R. Tchamango and A. Darchen, "bipolaires horizontales : effet de la structure des électrodes sur les performances du réacteur," vol. 6, pp. 4546–4554, 2018, doi: 10.1016/j.jece.2018.06.044.

[17] X. Chen, G. Chen, and P. L. Yue, "Separation of Pollutants from Restaurant Wastewater by Electrocoagulation.," *Sep. Purif. Technol.*, vol. 19, pp. 65–73, 2000, doi: http://dx.doi.org/10.1016/S1383-5866(99)00072-6.

[18] S. R. Tchamango, N. C. P., N. Emmanuel, H. Dimiter, and D. André, "Treatment of dairy ef fl uents by electrocoagulation using aluminium electrodes," *Sci. Total Environ. J.*, vol. 408, pp. 947–952, 2009, doi: 10.1016/j.scitotenv.2009.10.026.

[19] D. Lakshmanan and D. A. Clifford, "Ferrous and Ferric Ion Generation During Iron Electrocoagulation," *Environ. Sci. Technol*, vol. 43, no. 10, pp. 3853–3859, 2009.

[20] D. T. Moussa, M. H. El-naas, M. Nasser, and M. J. Al-marri, "A comprehensive review of electrocoagulation for water treatment : Potentials and challenges," *J Env. Manag.*, vol. 186, pp. 24–41, 2016, doi: 10.1016/j.jenvman.2016.10.032.

[21] F. Hussin, M. K. Aroua, and M. Szlachtac, "Combined solar electrocoagulation and adsorption processes for Pb(II) removal from aqueous solution," *Chem. Eng. Process. - Process Intensif.*, vol. 143, no. July, p. 107619, 2019, doi: 10.1016/j.cep.2019.107619.

[22] S. Elabbas *et al.*, "Eggshell adsorption process coupled with electrocoagulation for improvement of chromium removal from tanning wastewater," *Int. J. Environ. Anal. Chem.*, vol. 00, no. 00, pp. 1–13, 2020, doi: 10.1080/03067319.2020.1761963.

[23] S. Akter and M. S. Islam, "Effect of additional Fe2+ salt on electrocoagulation process for the degradation of methyl orange dye: An optimization and kinetic study," *Heliyon*, vol. 8, no. 8, Aug. 2022, doi: 10.1016/j.heliyon.2022.e10176.

[24] M. Y. Abdelnaeim, I. Y. El Sherif, A. A. Attia, and N. A. Fathy, "Impact of chemical activation on the adsorption performance of common reed towards Cu(II) and Cd(II)," *Int. J. Miner. Process.*, no. Ii, 2016, doi: 10.1016/j.minpro.2016.09.013.

[25] O. M. of A. AOAC, *Association of Official Analytical Chemists*, 18th ed. Washington DC., 2005.

[26] D. L. Kouadio, M. Diarra, A. C. Djassou, B. Dibi, B. K. Dongui, and K. Mamadou, "Etude expérimentale de l ' adsorption du bleu 16 et du méthyle rouge sur du charbon issu de la coque de la cabosse de cacao," *J. Soc. Ouest-Afr. Chim.*, vol. 051, pp. 17–30, 2022.

[27] Z. Khademi, B. Ramavandi, and M. Taghi, "Journal of Environmental Chemical Engineering The behaviors and characteristics of a mesoporous activated carbon prepared from Tamarix hispida for Zn (II) adsorption from wastewater," *Biochem. Pharmacol.*, vol. 3, no. 3, pp. 2057–2067, 2015, doi: 10.1016/j.jece.2015.07.012.

[28] J. Rodier, *L'analyse de l'eau*, 9e ed. Paris-France, 2009.

[29] S. De Gisi, G. Lofrano, M. Grassi, and M. Notarnicola, "Characteristics and adsorption capacities of low-cost sorbents for wastewater treatment: A review," *Sustain. Mater. Technol.*, vol. 9, pp. 10–40, 2016, doi: 10.1016/j.susmat.2016.06.002.

[30] C. Tcheka, M. Harouna, S. S. F. Gaineunbo, and M. Mbarki, "Kinetic and Equilibrium Studies on Adsorption of Methylene Blue and Methyl orange in Aqueous Solution onto Activated Carbon by H3PO4 Activation from the Hulls of Vitexdoniana," *Int. J. Innov. Appl. Stud.*, vol. 10, no. 1, pp. 101–108, 2015.

[31] M. Nassirou *et al.*, "Process conditions optimization of plant waste-derived microporous activated carbon using a full factorial design and genetic algorithm," *J. Mater. Environ. Sci.*, vol. 13, no. 8, pp. 884–899, 2022.

[32] S. D. B. Maazou, H. I. Hima, M. Mousbahou, M. Alma, and Z. Adamou, "Elimination of the chromium by the elaborate activated coal and characterized from the c-ockle of the core of Balanites Aegyptiaca," *Int. J. Biol. Chem. Sci.*, vol. 11, no. 6, pp. 3050–3065, 2017, doi: 10.4314/ijbcs.v11i6.39.

[33] R. Domga *et al.*, "Batch Equilibrium, Kinetic and Thermodynamic Studies on Adsorption of Methylene Blue in Aqueous Solution onto Activated Carbon Prepared from Bos Indicus Gudali Bones," *Chem. J.*, vol. 1, no. 6, pp. 172–181, 2015.

[34] A. Attour, N. Ben Grich, M. M. Tlili, M. Ben Amor, F. Lapicque, and J.-P. Leclerc, "Intensification of phosphate removal using electrocoagulation treatment by continuous pH adjustment and optimal electrode connection mode To cite this," *Desalin. Water Treat.*, 2022, doi: 10.1080/19443994.2015.1057537.

[35] H. Bacelo, A. M. A. Pintor, S. C. R. Santos, R. A. R. Boaventura, and C. M. S. Botelho, "Performance and prospects of different adsorbents for phosphorus uptake and recovery from water," *Chem. Eng. J.*, vol. 381, no. June 2019, p. 122566, 2020, doi: 10.1016/j.cej.2019.122566.

[36] K. M. Kifuani *et al.*, "Adsorption of basic dye, Methylene Blue, in aqueous solution on bioadsorbent from agricultural was from Cucumeropsis mannii Naudin," *Int. J. Biol. Chem. Sci.*, vol. 12, no. February, pp. 558–575, 2018.

[37] X. Liu and L. Zhang, "SC," *Powder Technol.*, 2015, doi: 10.1016/j.powtec.2015.02.055.

[38] C. Namasivayam and D. Sangeetha, "Equilibrium and kinetic studies of adsorption of phosphate onto ZnCl2 activated coir pith carbon," *J. Colloid Interface Sci.*, vol. 280, pp. 359–365, 2004, doi: 10.1016/j.jcis.2004.08.015.

[39] X. Liu *et al.*, "Biomass activated carbon supported with high crystallinity and dispersion Fe3O4 nanoparticle for preconcentration and effective degradation of methylene blue," *J. Taiwan Inst. Chem. Eng.*, vol. 81, pp. 265–274, Dec. 2017, doi: 10.1016/j.jtice.2017.10.002.

[40] F. Largo *et al.*, "Adsorptive removal of both cationic and anionic dyes by using sepiolite clay mineral as adsorbent: Experimental and molecular dynamic simulation studies," *J. Mol. Liq.*, vol. 318, 2020, doi: 10.1016/j.molliq.2020.114247.

[41] E. Lacasa, P. Ca, C. S áez, F. J. Fern ández, and M. A. Rodrigo, "Electrochemical phosphates removal using iron and aluminium electrodes," *Chem. Eng. J.*, vol. 172, pp. 137–143, 2011, doi: 10.1016/j.cej.2011.05.080.

[42] M. Chen, X. Li, Q. Zhang, C. Wang, H. Hu, and Q. Wang, "Phosphate removal from aqueous solution by electrochemical coupling siderite packed column," *Chemosphere*, vol. 280, no. May, p. 130805, 2021, doi: 10.1016/j.chemosphere.2021.130805.

[43] M. Kobya, P. Isaac, S. Mohammadzadeh, S. Yildirim, and Z. Ukundimana, "Phosphorous removal from anaerobically digested municipal sludge centrate by an electrocoagulation reactor using metal (Al, Fe and Al-Fe) scrap anodes," *Process Saf. Environ. Prot.*, vol. 152, pp. 188–200, 2021, doi: 10.1016/j.psep.2021.06.003.

[44] P. I. Omwene and M. Kobya, "Treatment of domestic wastewater phosphate by electrocoagulation using Fe and Al electrodes: A comparative study," *Process Saf. Environ. Prot.*, vol. 116, pp. 34–51, 2018.

[45] M. Kobya, E. Demirbas, N. U. Parlak, and S. Yigit, "Treatment of cadmium and nickel electroplating rinse water by electrocoagulation," *Environ. Technol.*, vol. 31, no. 13, pp. 1471–1481, 2010, doi: DOI: 10.1080/09593331003713693.

[46] N. Huda, A. A. A. Raman, M. M. Bello, and S. Ramesh, "Electrocoagulation treatment of raw landfill leachate using iron-based electrodes: Effects of process parameters and optimization," *J. Environ. Manage.*, vol. 204, pp. 75–81, Dec. 2017, doi: 10.1016/j.jenvman.2017.08.028.

[47] J. P. Kushwaha, V. C. Srivastava, and I. D. Mall, "Organics removal from dairy wastewater by electrochemical treatment and residue disposal," *Sep. Purif. Technol.*, vol. 76, no. 2, pp. 198–205, 2010, doi: 10.1016/j.seppur.2010.10.008.

[48] A. Eulmi, S. Hazourli, R. Abrane, M. Bendaia, A. Aitbara, and S. Touahria, "Evaluation of Electrocoagulation and Activated Carbon Adsorption Techniques Used Separately or Coupled to Treat Wastewater from Industrial Dairy," *Int. J. Chem. React. Eng.*, vol. 17, no. 12, pp. 1–12, 2019, doi: 10.1515/ijcre-2018-0229.

[49] Chow H. H., "The Removal Methods of Phosphorus/ Phosphate and Nitrogen/Nitrate from Water and Wastewater," Kuala Lumpur, 2012.